submitted to *Phys. Earth. Planet. Int.*

Modeling deformation rates in the Western Gulf of Corinth: rheological constraints

S. Cianetti, E. Tinti, C. Giunchi and M. Cocco

Istituto Nazionale di Geofisica e Vulcanologia, Sezione di Sismologia e Tettonofisica,

Via di Vigna Murata, 605, 00143 - Roma, ITALY.

22 March 2008

SUMMARY

The Gulf of Corinth is one of the most active extensional regions in the Mediterranean area characterized by a high rate of seismicity. However, there are still open questions concerning the role and the geometry of the numerous active faults bordering the basin as well as the mechanisms governing the seismicity. In this paper, we use a 2D plane strain finite element analysis to constrain the upper crust rheology by modeling the available deformation data (GPS and geomorphology). We consider a SSW-NNE cross-section of the rift cutting the main active normal faults (Aigion, West Eliki and Off-Shore faults) . The models run for 650 Kyrs assuming an elasto-visco-plastic rheology and 1.3 cm/yr horizontal extension as boundary condition (resulting from GPS data). We model the horizontal and vertical deformation rates and the accumulation of plastic strain at depth and we compare them with GPS data, with long term uplift rates inferred from geomorphology and with the distribution of seismicity, respectively. Our modeling results demonstrate that dislocation on high-angle normal faults in a plastic crustal layer plays a key role in explaining the extremely localized strain within the Gulf of Corinth. Conversely, the contribution of structures such as the antithetic Trizonia fault or the buried hypothetical sub-horizontal discontinuity are not necessary to model observed data.

Key words: Finite-element methods – Rheology – Normal faulting

1 INTRODUCTION

The western Gulf of Corinth (GOC) is one of the areas in the Mediterranean region showing the fastest extensional deformation rate. It is characterized by a high rate of shallow low-magnitude seismicity (Rigo *et al*. 1996; Harzfeld *et al*. 2000). However, several recent moderate magnitude earthquakes (5 events with $M_L \simeq 5.8$ in the last 35 years) ruptured offshore faults (Baker *et al*. 1997). Numerous recent investigations have been focused on the understanding of the rift evolution, mostly within different projects in the framework of the Corinth rift laboratory (CRL) (Bernard *et al*. 2006). GPS measurements collected during eleven temporary field campaigns performed between 1990 and 2001 show an extensional tectonics with an average value of the deformation velocity $\simeq$ 1.5 cm/year in the western and $\simeq$ 1.0 cm/year in the eastern part of the GOC, respectively. This suggests an increase in the opening rate from east to west due to the different rotation of the southern and northern blocks of the GOC (Avallone *et al*. 2004).

Some of the main normal faults outcropping in the western part of the GOC (see Fig. 1a), Aigion and West Eliki faults (hereinafter AIf and WEf, respectively), have been investigated in detail by geomorphological and paleoseismological observations (Palyvos *et al*. 2005; Pantosti *et al*. 2004) as well as by the Aigion drilling project in the framework of CRL (Cornet *et al*. 2004). These active faults exposed at the surface are quite steep (dipping at nearly 60°N and striking E-W) and mark the topography of the southern coast. The study of marine terraces (De Martini *et al*. 2004) provides a constraint to the uplift rate of southern shore ranging between 0.8 mm/yr and 1.3 mm/yr which corresponds to an upper bound of the fault slip-rate ranging between 4 to 7 mm/yr if an elastic dislocation model is used (De Martini *et al*. 2004).

The tectonic complexities of this area still prevent an exhaustive understanding of the mechanics of the rifting process: there is no general agreement concerning the geometry of crustal faults accommodating deformation and the rheology of the crust in this area is poorly known. Recently, an antithetic off-shore fault, the Trizonia fault (TZf) (see Fig. 1a) dipping $\sim 60^\circ$ to the south, has been also proposed as a consequence of the graben formation (Moretti *et al*. 2003; Bernard

et al. 2006). However, the role of the TZf in the rifting process is controversial and the geometry of the active faults located offshore is also debated. Some authors sustain the hypothesis that a nearly horizontal ($\sim 10°$) detachment (DEf) is active and drives the tectonic extension (Rigo *et al*. 1996; Briole *et al*. 2000; Sorel 2000; Bernard *et al*. 2006) causing the shallow seismicity. Other authors suggest that 8-12 km depth seismicity could be related to the brittle-ductile transition of the crust (Harzfeld *et al*. 2000). Chery (2001) proposes a mechanical model characterized by an elasto-visco-plastic crustal rheology in which the DEf (suspected to be inactive) corresponds to rotated, formerly active, high-angle faults. Moreover, studies of velocity structure reveal heterogeneities of the Moho depth along the GOC (Tiberi *et al*. 2001; Latorre *et al*. 2004; Zelt *et al*. 2005) that may have important implications for the lithospheric strength. Le Pourhiet *et al*. (2004) use a thermo-mechanical model to quantify the influence of rheological lateral heterogeneities on the development of fault patterns resulting from post-orogenic extension. They explain the observed microseismicity patterns, the asymmetry of the GOC and the kinematics of fault migration. However, they do not show any comparison with observed deformation rates. More recently, McNeill *et al*. (2005) strongly argue against the low angle DEf because it does not help to explain the observed extensional strain and its geometry is incompatible both with the off-shore faults cutting the entire seismogenic layer and with the majority of the fault plane solutions from microseismicity data.

Being aware of the complexity of the problem, we present a numerical model which accounts for all the available information, minimizing the assumptions and matching the observed data. Fig. 1b displays the geometry of the main faults considered in this study: the WEf, the AIf and the Off-shore (OSf) faults are all north-dipping, while the TZf is antithetic and south-dipping. The figure also shows the low angle structure which is interpreted either as an active DEf or as the brittle-ductile transition (Rigo *et al*. 1996; Harzfeld *et al*. 2000). We propose a simplified model using a 2D plane strain finite element (FE) approximation to simulate the evolution of the western part of the rift assuming a constant horizontal extension. Despite the use of a simplified model, we implement a non-linear rheology and include the plasticity condition; we account for the effects of fault interaction in a model with an assigned deformation rate. Our results are compared with

GPS velocities, recorded seismicity and uplift rates from geomorphology. The role of TZf and the buried low angle DEf will be discussed to understand their role in the rifting process.

2 NUMERICAL MODEL

The model is a 2D plane strain approximation of the SSW-NNE cross-section extending for 108 $\times$ 40 km across the GOC in the proximity of Aigion, a portion of the whole profile as shown in Fig. 1b. The AIf and OSf high angle normal faults are included in all the FE models. WEf, TZf and a low angle buried DEf are tested in some of the models. The geometry of the faults is taken from De Martini *et al*. (2004).

The mesh is discretized into 5817 four-node isoparametric elements. The finest resolution of $\simeq$ 300 m is near the pre-existing faults (Fig. 1) and decreases to $\simeq$ 2000 m along the mesh boundaries. The faults are modeled as deformable curves within the FE domain. Each side of the fault segment is described by a series of nodes connected by contact elements. These elements react to normal and shear tractions on the contact curves allowing us to account for frictional properties. In this paper we assume a Coulomb friction on the fault planes and, according to Chery (2001), a low effective static friction coefficient ($\mu = 0.1$). This assumption is justified both by modeling requirements and physical reasons. Indeed, we aim to model long–term deformation pattern and iterseismic GPS data; therefore we are not interested in modeling coseismic strain (i.e. earthquakes). Moreover, a low friction coefficient might be compatible with the presence of fluids that can control fault weakening mechanisms.

The initial stress distribution is characterized by a lithostatic stress ($\rho g z$) reference state (Engelder 1993). The model sinks due to the gravity load until the restoring force (characterized by a buoyancy stiffness ρg) applied at the base of the model sustains its weight. We assume that the GOC experienced a rapid extension of 1.3 cm/yr in the last 650 Kyrs in order to ensure 8 km opening (Chery 2001). Computations are performed with the Finite element commercial code MSC Software MARC 2005 Finite element analysis (2005).

The deformation pattern in the model is due to the contribution of elasto-plastic and creep strains. We define the same rheological properties over the whole domain, nonetheless, the as-

sumed temperature and the evolving stress and strain-rate conditions determine regions where elasto-plasticity dominates over thermally activated dislocation creep.

The hydrostatic stress dependence of brittle strength in crustal rocks is accounted by the elasto-plastic strain. This is determined according to the linear Drucker-Prager yield surface:

$$f = \alpha I_1 + \sqrt{J_2} - \frac{\bar{\sigma}}{\sqrt{3}} = 0, \tag{1}$$

where $I_1 = \sigma_{ii}$ is the first invariant of the stress tensor and $J_2 = \frac{1}{2}s_{ij}s_{ij}$ ($s_{ij} = \sigma ij - \frac{1}{3}I_1\delta_{ii}$) is the second invariant of the deviatoric stress tensor. The constants α and $\bar{\sigma}$ are related to the empirically determined Mohr-Coulomb parameters ϕ (internal friction angle) and C (cohesion) by the relations

$$sin\phi = \frac{3\alpha}{\sqrt{1-3\alpha^2}} \tag{2}$$

$$C = \frac{\bar{\sigma}}{\sqrt{3(1-12\alpha^2)}}. \tag{3}$$

The brittle to ductile transition due to temperature increase with depth is described by a time-dependent non–linear dislocation creep law . We compute the creep strain increment as a function of effective stress $\sigma = (\sigma_1 - \sigma_3)$ using the following expression:

$$\Delta\epsilon_c = A\sigma^n exp(-Q/RT)\Delta t \tag{4}$$

where A, Q and n are the pre-exponential, activation energy and exponent creep constants, respectively, while R is the gas constant (Brown and Phillips 2000). Creep parameters, shown in Table 1, are characteristic of continental lower crustal rocks (Wilks and Carter 1990). The absolute temperature T is computed by (Turcotte and Schubert 1982)

$$T(z) = T_0 + \frac{q_m}{k}z + \frac{\rho H_s {h_r}^2}{k}(1 - exp(-z/h_r)) \tag{5}$$

where T_0 is the surface temperature, $q_m = q_s - \rho H_s h_r$ the heat flow from mantle as a function of the heat flow at the surface, k the thermal conductivity, z is depth, ρH_s the radiogenic heat production and h_r the heat production scale depth. Parameters values, taken from Turcotte and Schubert (1982), are listed in Table 1 and the resulting geotherm is displayed in Fig. 2 for two different choices of q_s, as we will discuss in Section 3.1. This temperature distribution for GOC is consistent with previous thermo-mechanical models by Chery (2001) and Le Pourhiet *et al.*

(2004). Due to the short period examined we assume that the temperature does not change during the experiment: this condition allows us to perform a purely mechanical analysis.

In this paper we present a suite of seven models to understand the role of the different tectonic structures as well as the rheology of the crust in the GOC. All the models are characterized by the same boundary conditions: 1.3 cm/yr horizontal extension, buoyant force at the bottom, lithostatic initial stress and gravity load. The differences among the models are summarized in Table 2. We consider variations of both rheological (different plasticity and creep) and geometrical parameters (with/without WEf, TZf and DEf), and we also check the role of different activation times of the main faults.

3 MODELING DEFORMATION RATES

We show in Fig. 3 and Fig. 5 results from numerical simulations and we compare them with the GPS velocities measured during the 10 years time interval (Fig. 3a and 5a) and the long term uplift rate inferred from geomorphology indicated by the gray box in Fig. 3b and 5b. The predicted horizontal velocities (Fig. 3a and 5a) are computed averaging the calculated deformation over a 10 years time period corresponding to the time span of GPS measurements (Avallone *et al.* 2004). All the horizontal values are plotted in the Peloponnese reference frame. In our modeling we use 26 GPS stations by Avallone *et al.* (2004) whose distance from the cross section XX' of Fig.1, oriented N13°E, is less then $\sim$ 20 km. The uplift rates (Fig. 3b and 5b) are averaged over 500 Kyrs, since they are compared with the values inferred from longer term geomorphological estimates (De Martini *et al.* 2004; McNeill and Collier 2004) which span a similar time interval.

3.1 Effects of the rheology

The goal of this section is to investigate the rheological properties of the crust and to determine their compatibility with the GPS data recorded during geodetic campaigns. The horizontal velocity field inferred from GPS data (shown as solid circles in Fig. 3a) reveals that strain is quite localized in a limited area (less than 20 km wide) across the GOC, while to the south and to the north the crust behaves mostly as a rigid block. Unfortunately, the deformation is totally localized within the

GOC, that is below sea level, which limits the possibility to collect further data and to constrain the role played by active faults. For this reason we propose 4 models (summarized in Table 2) which can be considered as end members: M1 characterized by an elasto-viscous crustal layer, M2 and M3 which test the effects of plasticity parameters and finally M4 that shows the deformation rates obtained by imposing a colder geotherm (see Fig. 2 and Table 1) . In all these models only AIf and the OSf are assumed to be nowadays active and are included in the computations.

Fig. 3a shows that GPS data can not be reproduced by models characterized by an elastic crust: the horizontal velocity profile along the rift computed for the elasto-viscous model M1 (solid thin line) clearly shows a south to north linearly increasing trend. Moreover, the assumption of purely elastic deformation gives rise to unrealistic high differential stress in the crust (several GPa at the end of the computations). For these reasons, we select two models M2 (dashed line) and M3 (solid thick line), characterized by elasto-visco-plastic rheology with different values of cohesion C and internal friction angle ϕ (see Table 2). In Fig.4 we show the vertical profile of differential stress $(\sigma_1 - \sigma_3)$ in a target site located 5 km south of WEf; this figure shows that changing C and ϕ modifies the slope and the value of $(\sigma_1 - \sigma_3)$ at the surface for M2 and M3, leaving unchanged the depth of the brittle–ductile transition. The predicted horizontal velocity profiles for models M2 and M3 show an evident strain localization represented by the step-shaped extension within the GOC, in agreement with observed GPS data. It is clear that plasticity is the key mechanism to focus strain within the fault system while, north and south of the GOC, the crust is only slightly deformed. Predictions from M2 and M3 are characterized by small differences that lie within data uncertainties. Maximum differential stress accumulated in the crust is, for these two models, of the order of 200–300 MPa, less than values obtained from simulations with elastic crust. We also consider variations of the thermal activated creep, which determines the strength of the crust below the plasticity yield stress, considering model M4 (Fig. 3a, dotted line). We assume a surface heat flow q_s as low as 50 mW m^{-2}, extrapolating to the whole GOC the measure obtained for the AIf (Doan and Cornet 2007). In this case, creep for M4 develops at larger depth with respect to M2 and M3, as shown in Fig. 4 (dotted line), and the plastic regime extends accordingly, but the horizontal surface deformation rate is still quite similar to M2 and M3.

We have verified that the discrimination among the end member models M2, M3 and M4 is very difficult only considering the horizontal deformation rate (also due to the large GPS data uncertainties). Unfortunately, GPS vertical rates have not been measured with sufficient accuracy to be significant (Avallone *et al*. 2004). For this reason, in Fig. 3b we compare the long-term vertical deformation rate of the proposed models with the geomorphological estimate by De Martini *et al*. (2004) and with the observation that the northern part of the GOC has been subject to reduced uplift. Model M1 shows a lowered slip of AIf and OSf and a longer wavelength deformation rate with respect to models M3-M4. Again, we emphasize the role of plasticity to obtain small scale features in the deformation rate profiles. Among plastic models, M2 and M4 predict rather symmetrical uplift rates on the north and south sides of the GOC, while M1 and M3 are more asymmetric focusing the uplift rate on the southern part. However, the predicted uplift rates are smaller than the geomorphological estimate (gray box in Fig. 3b) for any model but M1 and M3, which better match the proposed long term uplift rates. In the following we therefore use the rheological model M3 as the most representative one, since it is compatible both with the horizontal and with vertical deformation rates.

3.2 Effects of the faults activity

In the previous section we have shown how variations of rheological properties affect the predicted deformation rates. In this section we keep fixed the rheological parameters of model M3 and we investigate the role of the activation of different faults. In particular we take into account the activation of: DEf (M3D); TZf (M3TZ); AIf, OSf and WEf at different times (M3T).

One important issue concerns the existence and the role of the buried low angle DEf at the base of the high angle shallow faults bordering the GOC. It is still unclear if it is a physical discontinuity or a rheological effect. On one hand, McNeill *et al*. (2005) conclude that a low angle DEf is superfluous to match extensional strain and is also incompatible with microseismicity data. On the other hand, Briole *et al*. (2000) and Bernard *et al*. (2006) simulate the regional tectonic load in terms of slip on this low angle DEf, which is embedded in an elastic homogeneous half-space

and extends semi–infinitely in the downdip direction. In this study we also propose a model in which DEf is considered an active fault (model M3D, dashed line in Fig. 5).

By comparing models M3 and M3D, only differing for the presence of DEf, we note in Fig. 5a that M3D yields a deformation pattern spreaded in a broader area, while slip rate on AIf and OSf increases with respect to M3. In Fig. 5b we observe that model M3D yields predictions in the southern part of the GOC comparable to geologic estimates ranging between 0.8 and 1.3 cm/yr (De Martini *et al*. 2004; McNeill and Collier 2004), but it also predicts significant uplift in the northern part. Slip rates on AIf and OSf resulting from model M3 are 2.7 mm/yr and 1.8 mm/yr, respectively, while for M3D are 3.3 mm/yr and 2.5 mm/yr, respectively. This means that the presence of the low angle structure affects the activity of the high-angle normal faults. Analyzing model M3D, we find that the slip-rate on DEf is small (no larger than 0.6 mm/yr) and confined just below the shallow active normal faults, while vanishes elsewhere. Therefore, our simulations suggest that the low angle discontinuity DEf only accommodates a small amount of deformation and, if it exists, it is of secondary importance with respect to AIf and OSf. We have also verified this statement testing a model where DEf is the only active fault: in this case no slip is observed on DEf. This allows us to conclude that motion on this fault, if present, is controlled and promoted by slip on the high angle dipping faults.

Several papers in the recent literature (Moretti *et al*. 2003; Bernard *et al*. 2006) focus on the role of TZf, which is considered by these authors as an active structure accommodating crustal extension. Solid thin lines in Fig. 5a,b show the model M3TZ, where TZf is considered as a main structure accommodating the deformation in the study area simultaneously with AIf and OSf. Horizontal velocity predictions still have similarities with other models but in the southern part of the GOC they overestimate geodetic data (predicting 0.25 cm/yr). North of the GOC the fit improves with respect to the southern area and predicted velocities are within data uncertainties. Uplift rate (Fig. 5b) is characterized by a symmetric profile between the northern and southern rims of the GOC due to the presence of the antithetic TZf. We speculate that this should imply an unrealistic shape of the topographic relief, suggesting that the role of TZf to accommodate crustal extension in this region is subordinate to the other high angle normal faults.

Finally, we take into account a model to address the effects of the past activity of the WEf on the present-day deformation rate: although this fault might be presently not active anymore (Pantosti *et al*. 2004), there is evidence that it played a major role in controlling the GOC opening in the past (De Martini *et al*. 2004). We perform a simulation (model M3T, dotted line in Fig. 5) taking into account the progressive activation of the three major north-dipping normal faults (WEf, AIf and OSf). We impose a temporal constraint on WEf and AIf activity according to De Martini *et al*. (2004) and McNeill *et al*. (2007): WEf is the first to be active, until 250 Kyrs ago and being temporally overlapped by AIf in the last 50 Kyrs of its activity. Afterwards AIf is the only active fault, until 50 Kyrs when also OSf becomes active. We are aware that these are very indicative ages, but we are confident that even relatively uncertainties in their estimation do not significantly affect the results. Indeed, we find that present-day estimate of opening rate is only partially affected by these assumptions (see Fig. 5a), the rifting being spread over a wider area south of the GOC. The stronger effect can be seen in Fig. 5b, since the progressive activation of the sub-parallel north-dipping normal faults extends the positive uplift rate to the south and to the north with respect to all the other models in which WEf activity is not taken into account. Moreover, the uplift rate profile just south of the GOC is now characterized by a maximum in the proximity of WEf and by a second relative maximum contiguous to AIf. Uplift rates are, in any case, lower that geomorphology estimates. The slip-rates for AIf, WEf and OSf are 2.3 mm/yr, 2.1 mm/yr and 1.8 mm/yr, respectively.

4 COMPARISON WITH SEISMIC ACTIVITY

In this section we conclude our analysis discussing the recent seismic activity recorded nearby the study area to understand how it is related to the present-day active deformation pattern. In Fig. 6a we plot the relocated seismic events (occurred on 2000-2004; Lyon Caen personal communication) in a vertical, N13°E, cross section with a magnitude greater than 1.2 and a distance from the section lower than 4 km. In the literature different mechanical models have been proposed to explain this low-magnitude, shallow and diffuse seismicity (Rigo *et al*. 1996; Sorel 2000; Bernard *et al*. 2006; Harzfeld *et al*. 2000; Chery 2001; McNeill *et al*. 2007). Here we map the

total equivalent plastic strain, computed for the two numerical models (M3 and M3D in Fig. 6b-c, respectively) selected on the basis of the fit to the available data. This quantity identifies regions where significant yielding or shear dislocation on pre-existing faults have occurred: it is likely to expect that either new fractures are formed in these areas or damage develops around existing discontinuities. However, the elasto-visco-plastic rheology does not allow us to assess whether or not in such zones seismic events will effectively occur. Indeed, the plasticity equation (1) is not able to distinguish between stable and unstable slip (Albert and Phillips 2002) because we do not use a fracture criterion neither a constitutive frictional law, in the modeled volume, which would allow us the proper description of dynamic instabilities. The concentration of plastic strain in certain areas can be considered as a necessary but insufficient condition for promoting seismicity. A more suitable crustal rheology, based on damage mechanics, would be more appropriate to model the seismicity patterns (Hamiel *et al*. 2004).

The pattern of total equivalent plastic strain for model M3 and model M3D is shown in Fig. 6b-c, respectively. Dashed lines, in each panel, represent the faults assumed to be not active. It is evident how the laterally homogeneous rheology condition, imposed at the starting time for all the models, is perturbed by the presence of active faults. In both models, plastic strain accumulates at the wedge-shaped area enclosed between OSf and TZf (the latter being considered in both cases inactive), where no seismicity has been recorded. The location of TZf coincides with the northern bound of this enhanced plastic strain region, whose extension is controlled by the dip, location and length of AIf and OSf. On the one hand, the presence of this plastic deformation is consistent with the observed surface breakage proposed by (Moretti *et al*. 2003); on the other, the lack of seismicity does not allow us to constrain and verify the activity of this fault at depth. Our interpretation is that the accumulation of deformation in this area might promote the developing of an antithetic fault, but this does not imply that TZf will be able to generate moderate-to-large earthquakes.

Plastic strain concentrations are also found in proximity of AIf and OSf roots, where microseismicity is clustered between 5 and 8 km depth. In this case plastic strain and microseismicity could be akin to the presence of highly fractured rocks (due to repeated dislocations on the planes of the main faults). This interpretation is also consistent with the evidence of fault plane solutions,

for earthquakes at this depth, not related to the geometry of the proposed DEf plane (Harzfeld *et al*. 2000). The seismicity at depth is not limited to the terminations of OSf and AIf, but it extends also to the north of TZf with a slight increase of hypocenters depth. Both models shown in Fig. 6 fail in predicting an evident increase of total equivalent plastic strain in this zone. In particular, model M3D concentrates more plastic strain than M3 below DEf (i.e. in its footwall), while the area where seismicity is clustered remains almost totally undeformed in our simulations. Our computations suggest that model M3D does not provide a better match to observed seismicity than model M3. The mismatch between plastic strain and observed seismicity below TZf can be due either to an inaccurate representation of faults geometry at depth or to the effects of secondary mechanisms triggering seismicity. In the former case, the active fault system might be characterized either by the presence of additional north-dipping normal faults located off-shore (consistent with the northward migration of active deformation in the GOC) or by a listric geometry at depth (but we tend to discard this second hypothesis because of the results of model M3D). In the latter case, seismicity might be caused by poroelastic relaxation processes promoted by plastic deformation and fluid flow. In other words, we speculate that the observed seismicity pattern might be caused by inelastic off-fault response enhanced by fluid pressurization (Jónsson *et al*. 2003; Fialko 2004; Poliakov *et al*. 2002; Miller *et al*. 2004). While our modeling results are not exhaustive, we suggest that evidence for an active low angle DEf is not robust and not corroborated by data modeling.

5 CONCLUSIONS

The GOC is one of the best monitored and studied area in the Mediterranean region; however, the present state of knowledge concerning the crustal rheological parameters is still insufficient to constrain detailed numerical models. In this paper, we face this problem trying to explain the observed active deformation assuming a model in which the geometry is simplified but the crustal rheology is quite realistic, including plasticity and nonlinear creep. We are aware that the deformation mechanisms of the discussed models are characterized by a time scale much longer than that one sampled by geodetic and seismic campaigns. This means that the snapshots taken from the models evolution and used for the comparison with observed data might not include short time

scale events (i.e., large earthquakes) whose signals have been removed from the observed data (Avallone *et al*. 2004). For example, seismic activity recorded from 2000 to 2004 in the GOC can be also promoted by stress perturbations caused by moderate-magnitude earthquakes occurred in the 90s, and not solely generated by the active deformation following the rifting process. In other words, our modeling results allow us to constrain a cumulative long term slip rate on active faults, but we cannot constrain its partitioning between creeping and coseismic slip episodes.

Despite these simplistic assumptions, our results provide an interpretation of the extremely localized strain-rate and allow us to obtain an acceptable fit to observed data. We emphasize that plasticity of the shallow crust is an essential ingredient to explain strain localization. We summarize here the following conclusions: *(i)* high angle normal faults embedded in an elasto-plastic layer are necessary to localize deformation in a small area across the GOC, as shown by the horizontal velocity data; *(ii)* the terminations at depth of these faults are responsible for the development of enhanced plastic strain volume in the proximity of TZf; *(iii)* as a consequence, the activity on TZf is not required to reproduce observed deformation rates and the proposed surface breakage on TZf might be associated with the effects of plasticity near the Earth surface; *(iv)* the comparison with surface deformation rates inferred from GPS data does not allow us to discriminate whether the low angle DEf is active or not. However, the presence of an active detachment makes difficult the interpretation of observed seismicity in terms of plastic strain accumulation; *(v)* only few models are simultaneously compatible both with observed horizontal opening rates and long term uplift rates inferred from geology; *(vi)* slip rates on active faults are smaller than upper bound estimates obtained by elastic dislocation models used to interpret geomorphology.

Finally, we remark that models can be certainly improved by more accurate geometry of AIf and OSf as well as by a more refined crustal rheology. Nevertheless, better constrained model would require an improvement in the quantity and quality of available data.

ACKNOWLEDGMENTS

We thank D. Pantosti, P.M. De Martini, D. La Torre, P. Briole, J. Chery and M. Bonafede for useful discussions. We are grateful to A. Avallone for GPS data and to H. Lyon-Caen for seismicity data.

E. Tinti was partially supported by the EC grant 3HAZ-Corinth research project 04043 (GOCE). The paper benefited from constructive reviews of the editor Y. Ben-Zion and two anonymous referees.

REFERENCES

Albert, R. A. & R. J. Phillips, 2002. Time-dependent effects in elastoviscoplastic models of loaded lithosphere, *Geophys. J Int.*, **151**, 612–621.

Avallone, A., Briole, P., Agatza-Balodimou, A.M., Billiris, H., Charade, O., Mitsakaki, C., Nercessian, A., Papazissi, K., Paradissis, D. & G. Veis, 2004. Analysis of eleven years of deformation measured by GPS in the Corinth Rift Laboratory area, *Comptes Rendus Geoscience*, **336**, 301–311, doi:10.1016/j.crte.2003.12.007.

Baker, C., Hatzfeld, D., Lyon-Caen, H., Papadimitriou, E. & A. Rigo, 1997. Earthquake mechanisms of the Adriatic Sea and Western Greece: Implications for the oceanic subduction-continental collision transition,*Geophys. J Int.*, **131**, 559–594.

Bernard, P., Lyon-Caen, H., Briole, P., Deschamps, A., Boudin, F., Makropoulos, K., Papadimitriou, P., Lemeille, F., Patau, G., Billiris, H., Paradissis, D., Papazissi, K., Castarede, H., Charade, O., Nercessian, A., Avallone, A., Pacchiani, F., Zahradnik, J., Sacks, S. & A. Linde, 2006. Seismicity, deformation and seismic hazard in the western rift of Corinth: New insights from the Corinth Rift Laboratory (CRL), *Tectonophysics*, **426**, 7–30, doi:10.1016/j.tecto.2006.02.012.

Hamiel, Y., Liu, Y., Lyakhovsky, V., Ben-Zion, Y. & D. Lockner, 2004. A viscoelastic damage model with application to stable and unstable fracturing, *Geophys. J Int.*, **159**, 1155–1165, doi:10.1111/j.1365-246X.2004.02452.x.

Briole, P., Rigo, A., Lyon-Caen, H., Ruegg, J. C., Papazissi, K., Mitsakaki, C., Balodimou, A., Veis, G., Hatzfeld D. & A. Deschamps, 2000. Active deformation of the Corinth Rift, Greece: results from repeated Global Positioning System survey between 1990 and 1995, *J. geophys. Res.*, **105**, 25,605–25,625.

Brown, C. D., & R. J. Phillips, 2000. Crust–mantle decoupling by flexure of continental lithosphere, *J. geophys. Res.*, **105**, 13,221–13,237

Chery, J., 2001. Core complex mechanics: From the Gulf of Corinth to the Snake Range, *Geology*, **29**, 439–442.

Cornet, F.H., Doan, M.L., Moretti, I. & G. Borm, 2004. Drilling through the Aigion fault: The AIG10 well observatory, *Comptes Rendus Geoscience*, **336**, 395–406, doi:10.1016/j.crte.2004.02.002.

De Martini, P. M., D. Pantosti, N. Palyvos, Lemeille, F., McNeill, L. & R. Collier. 2004. Slip rates of the Aigion and Eliki faults from uplifted marine terraces, Corinth Gulf, Greece, *Comptes Rendus Geoscience*, **336**, 325–334, doi:10.1016/j.crte.2003.12.006.

Doan, L. M. & F. H. Cornet, 2007. Thermal anomaly near the Aigio Fault, Gulf of Corinth, Greece, maybe due to convection below the fault, *Geophys. Res. Lett.*, **34**, L06314, doi:10.1029/2006GL028931.

Engelder, T., 1993. *Stress Regimes in the Lithosphere*, Princeton University Press, Princeton, NJ.

Fialko, Y., 2004. Evidence of fluid–filled upper crust from observations of post–seismic deformation due to the 1992 M_w 7.3 Landers earthquake, *J. geophys. Res.*, **109**, B08401, doi:10.1029/2003JB001985.

Harzfeld, D., Karakostas, V., Ziazia, M., Kassaras, I., Papadimitriou, E., Makropoulos, K., Voulgaris, N. & C. Papaioannou, 2000. Microseismicity and faulting geometry in the Gulf of Corinth (Greece), *Geophys. J Int.*, **141**, 438–456.

Jónsson, S., Segall, P., Pedersen, R. & G. Björnsson, 2003. Post–earthquake ground movements correlated to pore–pressure transients, *Nature*, **424**, 179–183.

Le Pourhiet, L., Burov, E. & I. Moretti, 2004. Rifting through a stack of inhomogeneous thrusts (the dipping pie concept), *Tectonics*, **23**, TC4005, doi:10.1029/2003TC001584.

Latorre, D., Virieux, J., Monfret, T., Monteiller, V., Vanorio, T., Got, J. L. & H. Lyon-Caen, 2004. A new seismic tomography of Aigion area (Gulf of Corinth, Greece) from the 1991 data set, *Geophys. J Int.*, **159**, 1013–1031, doi:10.1111/j.1365-246X.2004.02412.x.

AA.VV., 2005. Theory and Users information, Palo Alto, CA.

McNeill, L. & R. E. LL. Collier, 2004. Uplift and slip rate of the eastern Eliki fault segment, Gulf of Corinth, inferred from Holocene and Plesticene terraces, *J. Geol. Soc.*, **161**, 81–92.

McNeill, L., Cotterill, C. J., Henstock, T. J., Bull, J. M., Stefatos, A., Collier, R. E. LI., Papatheoderou, G., Ferentinos G. & S. E. Hicks, 2005. Activity faulting within the offshore western Gulf of Corinth, Greece: implications for models of continental rift deformation, *Geology*, **33**, 241–244, doi:10.1130/G21127.1.

McNeill, L., Cotterill, C. J., Bull, J. M., Henstock, T. J.,Bell, R. & A. Stefatos, 2007. Geometry and slip rate of the Aigion fault, a young normal fault system in the western Gulf of Corinth, *Geology*, **35**, 355–358, doi:10.1130/G23281A.1.

Miller, S. A., Collettini, C., Chiaraluce, L., Cocco, M., Barchi M. & B. J. P. Kaus, 2004. Aftershocks driven by a high-pressure CO (sub 2) source at depth, *Nature* ,**427**, 724–727.

Moretti, I., Sakellariou, D., Lykousis, V. & L. Micarelli, 2003. The Gulf of Corinth: an active half graben?,*Journal of Geodynamics*, **36**, 323–340.

Okada, Y., 1992. Internal deformation due to shear and tensile faults in a half-space, *Bull. seism. Soc. Am.*, **82**, 1018–1040.

Palyvos, N., Pantosti, D., De Martini, P.M., Lemeille, F., Sorel D. & K. Pavlopoulos, 2005. The Aigion-Neos Erineos coastal normal fault system (Western Corinth Gulf rift, Greece): Geomorphological signature, recent earthquake history and evolution, *J. geophys. Res.*, **110**, B09302, doi:10.1029/2004JB003165.

Pantosti, D., De Martini, P.M., Koukouvelas, I., Stamatopoulos, L.,Palyvos, N., Pucci, S., Lemeille, F. & S. Pavlides, 2004. *Comptes Rendus Geoscience*, **336**, 335–342, doi:10.1016/j.crte.2003.12.005.

Poliakov A. N. B., Dmowska R. & J. R. Rice, 2002. Dynamic shear rupture interactions with fault bends and off-axis secondary faulting, *J. geophys. Res.*, **107**, doi:10.1029/2001JB000572.

Rigo, A., Lyon-Caen, H., Armijo, R., Deshamps, A., Harzfeld, D., Makropoulos, K., Papadimitriou P. & I. Kassaras, 1996. A microseismic study in the western part of the Gulf of Corinth (Greece): implications for large-scale normal faulting mechanisms, *Geophys. J Int.*, **126**, 663–688.

Sorel, D., 2000. A Pleistocene and still-active detachment fault and the origin of the Corinth-Patras rift, Greece, *Geology*, **128**,(1) 83–86.

Tiberi, C., Diament, M.. Lyon-Caen, H. & T. King, 2001. Moho topography beneath the Corinth Rift area (Greece) from inversion of gravity data, *Geophys. J Int.*, **145**,(3), 797–808.

Turcotte D. L. & G. Schubert, 1982. *Geodynamics - Application of continuum physics to geological problems*, Wiley, New York.

Wilks, K. R. & N. L. Carter, 1990. Rheology of some continental lower crustal rocks, *Tectonophysics*, **182**, 57–77.

Zelt B.C., Taylor, B., Sachpazi, M. & A. Hirn, 2005. Crustal velocity and Moho structure beneath the Gulf of Corinth, Greece, *Geophys. J Int.*, **162**,(1), 257–268.

Table 1. Rheological Parameters

Parameter	Symbol	Value
Young's modulus	E	26 GPa
Poisson ratio	ν	0.3
Density	ρ	3000 kg m^{-3}
Gravity	g	10 m s^{-2}
Cohesion	C	10, 50 MPa
Internal friction coefficient	ϕ	20°, 30°
Effective static fault friction	μ	0.1
Activation energy	Q	243 KJ mol^{-1}
creep exponent	n	3.1
Pre-exponential constant	A	8×10^{-3} MPa^{-n} s^{-1}
Surface temperature	T_0	273 ° K
Thermal conductivity	k	3.35 W m^{-1} K^{-1}
Surface heat flow	q_s	50, 60 mW m^{-2}
Radiogenic heat production	ρH_s	1 μW m^{-3}
Heat production scale depth	h_r	10 km

Table 2. Models summary

Model	Active faults	C (MPa)	ϕ	q_s (mW m^{-2})
M1	AIf, OSf	–	–	60
M2	AIf, OSf	10	20°	60
M3	AIf, OSf	50	30°	60
M4	AIf, OSf	50	30°	50
M3TZ	AIf, OSf,TZf	50	30°	60
M3D	AIf, OSf, DEf	50	30°	60
M3T	AIf, OSf,WEf	50	30°	60

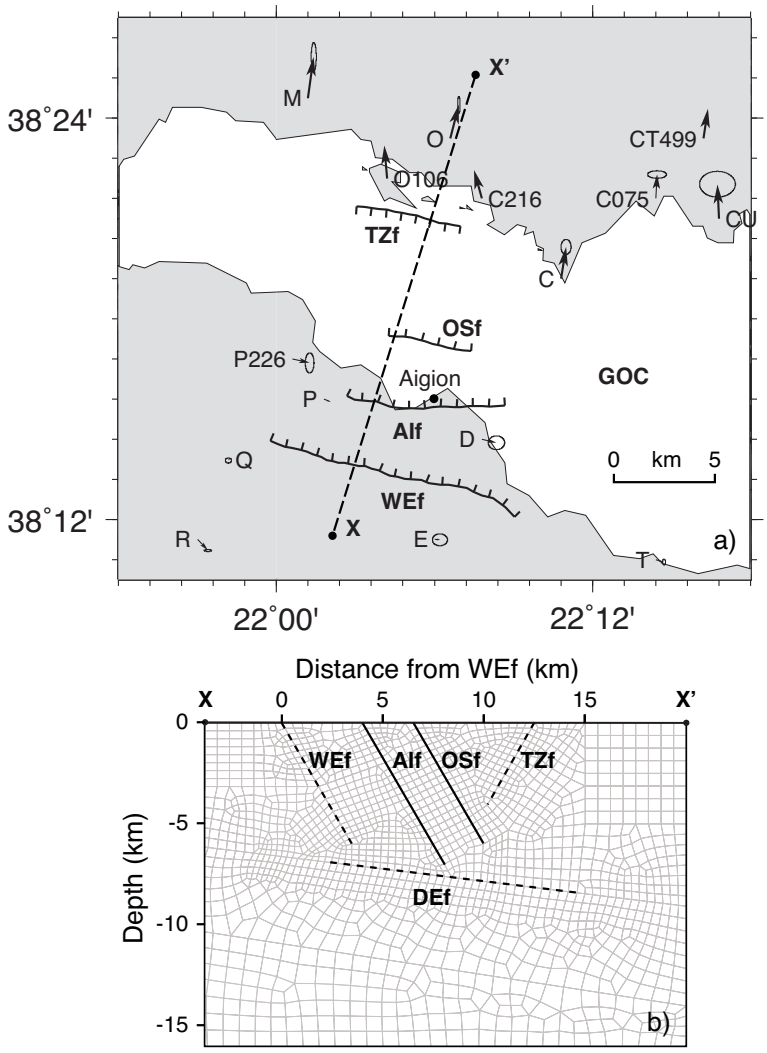

Figure 1. a) Map of the Western Gulf of Corinth (GOC) showing the position of the main high angle normal faults integrated in the models: West Eliki (WEf), Aigion (AIf), Off-Shore (OSf) and Trizonia (TZf). Black arrows are GPS velocities plotted in the Peloponnese reference system Avallone *et al*. (2004). The total number of GPS stations is 26 while in this figure only the area closer to the active faults is displayed. X-X' indicates the horizontal trace of the modeled vertical cross-section. b) Vertical cross-section along the X-X' profile showing a subset of the finite element grid near the modeled faults. Solid lines show the faults always included in the computations, while dashed lines are for discontinuities tested in selected models. DEf is the low angle detachment.

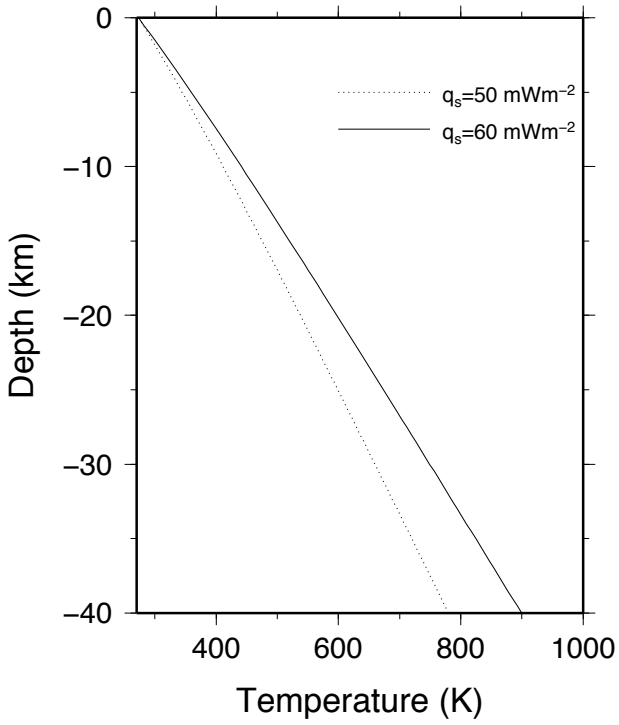

Figure 2. Temperature profiles considered in this study

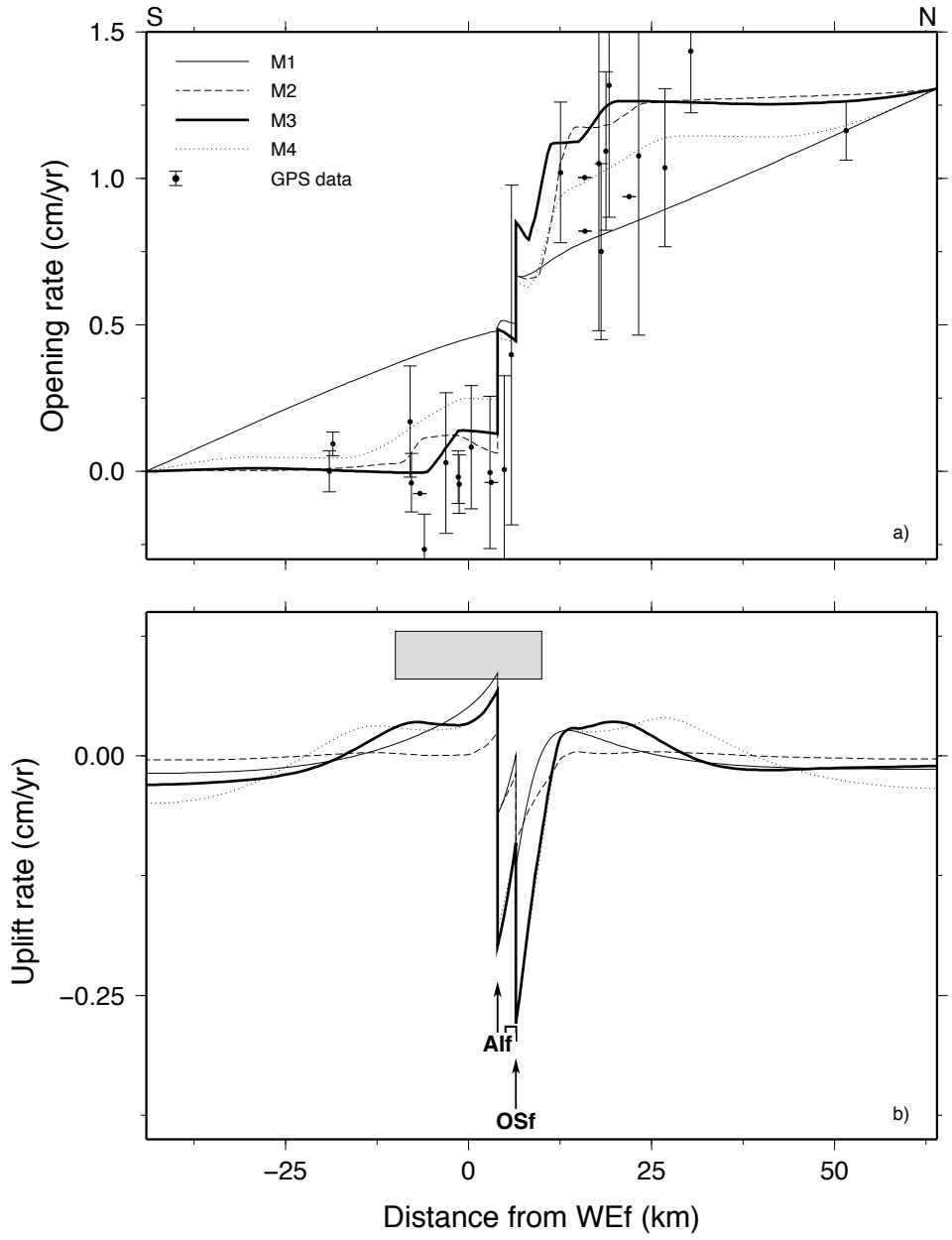

Figure 3. a) Horizontal velocities with error bars measured from GPS data whose distance from the model are less than $\sim$ 20 km, are plotted in the Peloponnese reference system. These are compared with the opening rate computed for models characterized by different rheologies (see Table 2 for details). b) Uplift rates are compared with the long term uplift rate inferred from geomorphology (shown as gray shaded box).

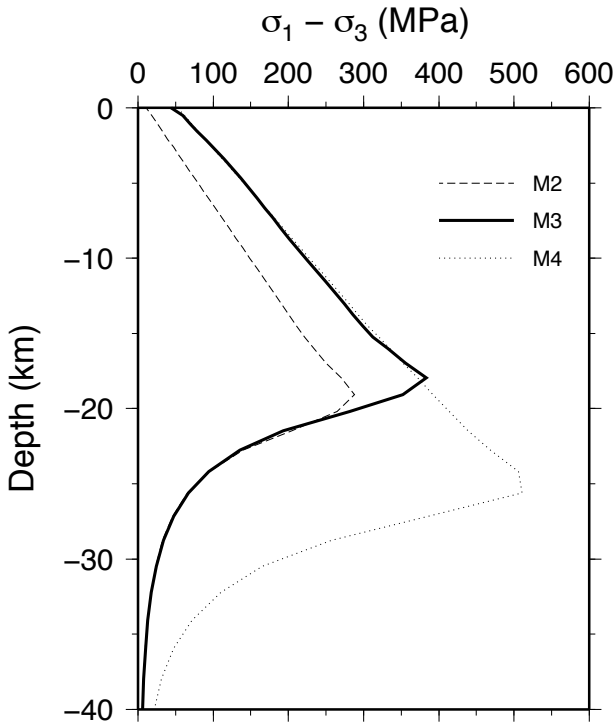

Figure 4. Differential stress as a function of depth for model M2 (dashed), M3 (solid) and M4 (dotted)

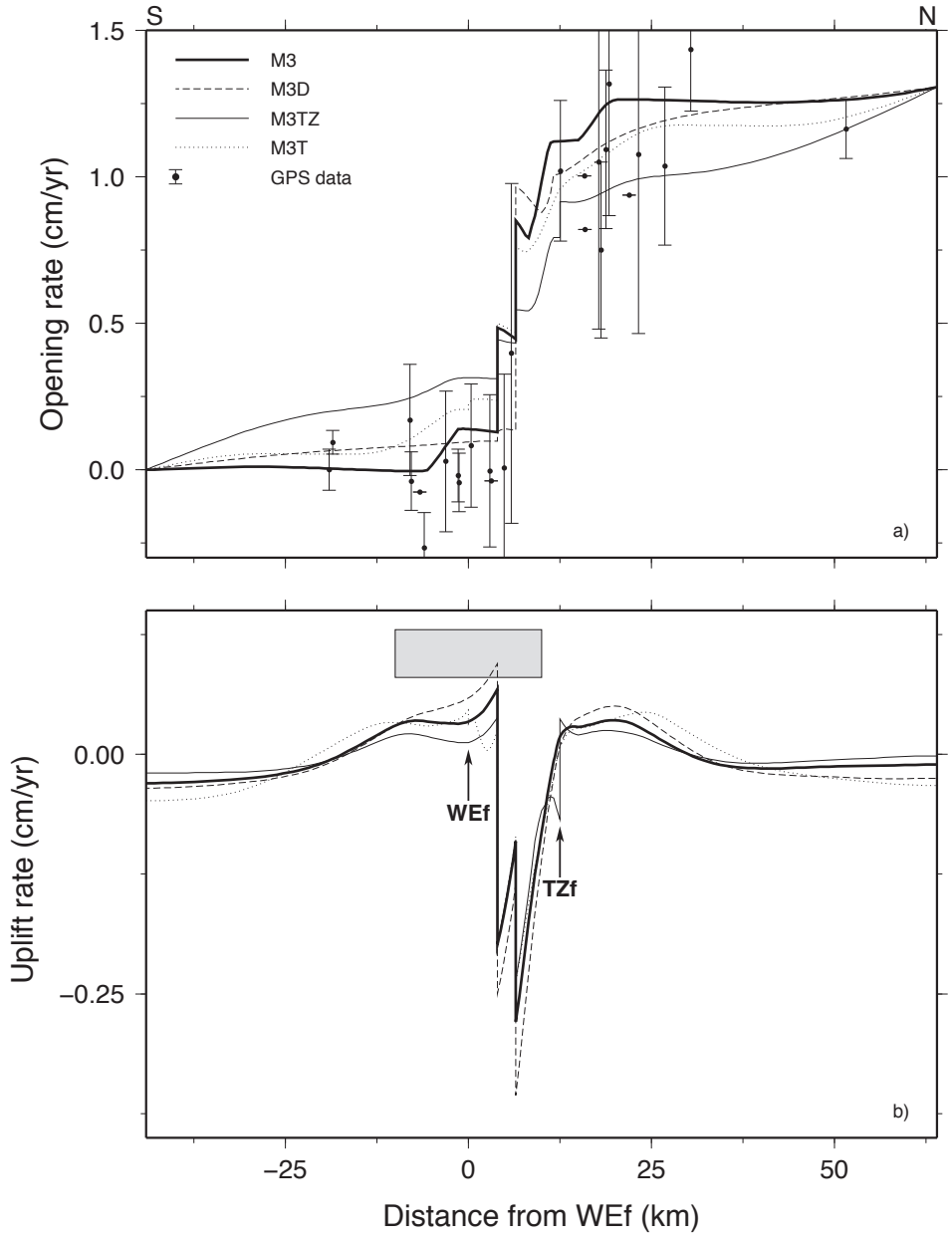

Figure 5. Same as in Fig. 3 but for models characterized by the same rheology of model M3 and different active faults.

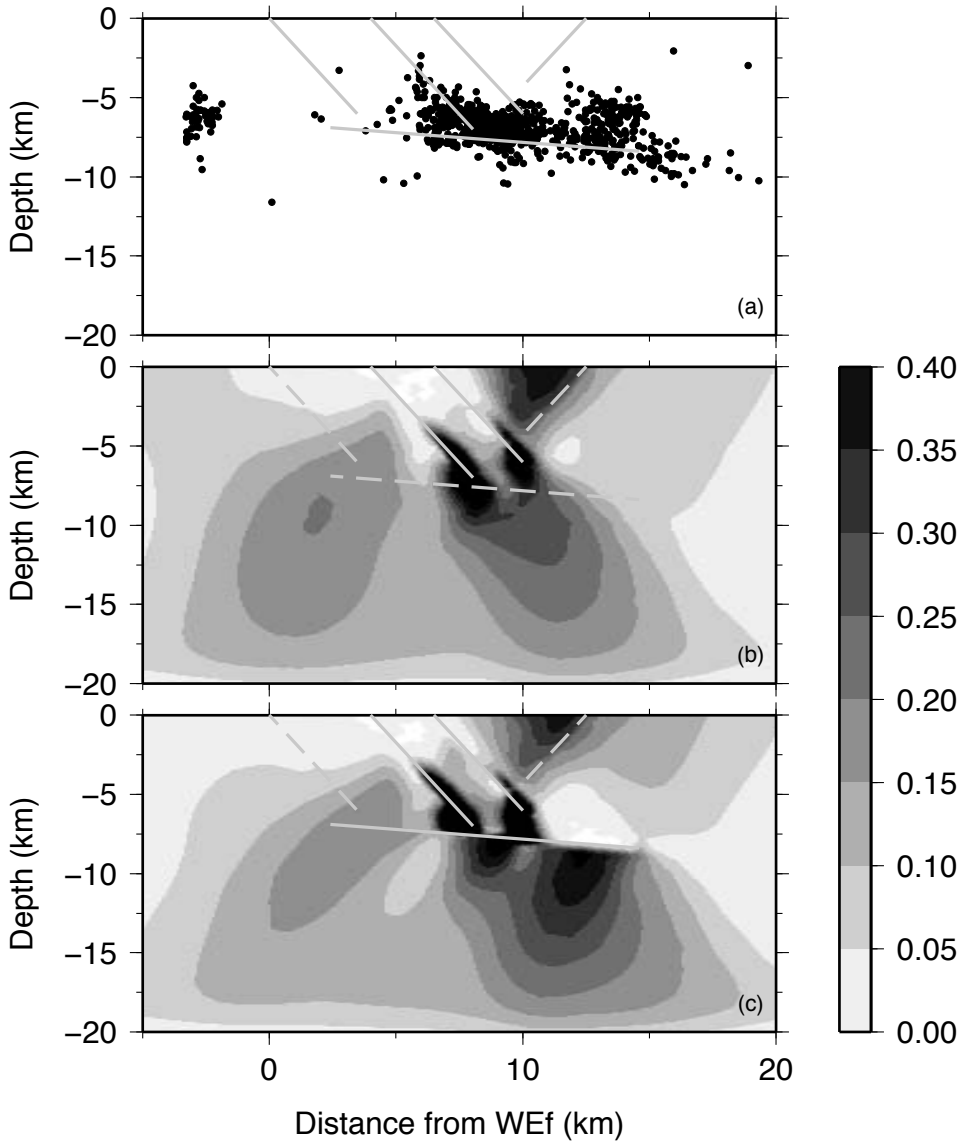

Figure 6. a) Black circles show relocated events of the time period 2000-2004 (Lyon Caen, personal communication) whose distance; b)-c) Contour bands display the total equivalent plastic strain at the end of computations for models M3 and M3D. Fault traces are shown as gray lines: solid for active and dashed for inactive faults, respectively.